A multi-level model analysis of lipolysis and fatty acid release from adipocytes *in vitro* and from adipose tissue *in vivo*

William Lövfors[1,2], Jona Ekström[1], Cecilia Jönsson[3], Peter Strålfors[3], Gunnar Cedersund[1,4], and Elin Nyman[1*]

[1]Department of Biomedical Engineering, Linköping University, Linköping, Sweden
[2]Department of Mathematics, Linköping University, Linköping, Sweden
[3]Department of Biomedical and Clinical Sciences, Linköping University, Linköping, Sweden
[4]Center for Medical Image Science and Visualization (CMIV), Linköping University, Linköping, Sweden
[*]Corresponding author, elin.nyman@liu.se, +46 13 286712, Department of Biomedical Engineering, Linköping University, 58183 Linköping, Sweden

Lipolysis and the release of fatty acids to supply energy to other organs, such as between meals, during exercise, and starvation, are fundamental functions of the adipose tissue. The intracellular lipolytic pathway in adipocytes is activated by adrenaline and noradrenaline, and inhibited by insulin. Circulating fatty acids are elevated in type 2 diabetic individuals. The mechanisms behind this elevation are not fully known, and to increase the knowledge a link between the systemic circulation and intracellular lipolysis is key. However, data on lipolysis and knowledge from *in vitro* systems have not been linked to corresponding *in vivo* data and knowledge *in vivo*. Here, we use mathematical modelling to provide such a link. We examine mechanisms of insulin action by combining *in vivo* and *in vitro* data into an integrated mathematical model that can explain all data. Furthermore, the model can describe independent data not used for training the model. We show the usefulness of the model by simulating new and more challenging experimental setups *in silico*, e.g. the extracellular concentration of fatty acids during an insulin clamp, and the difference in such simulations between individuals with and without type 2 diabetes. Our work provides a new platform for model-based analysis of adipose tissue lipolysis, under both non-diabetic and type 2 diabetic conditions.

List of abbreviations: cAMP – cyclic adenosine monophosphate; IR – insulin receptor; PKB – protein kinase B; PDE3B – phosphodiesterase 3B; AR – adrenergic receptor; HSL – hormone-sensitive lipase; AC – adenylyl cyclase; T2D – type 2 diabetes ODE – ordinary differential equation

Introduction

Lipolysis, the breakdown of triacylglycerol to glycerol and fatty acids, and the subsequent release of the fatty acids and glycerol as energy fuel for other organs, is one of the main functions of the adipose tissue. Because of the critical role of fatty acids as a fuel for the body, this function is also central to energy homeostasis. Interest in lipolysis has gained more traction as the prevalence of obesity, type 2 diabetes and its sequelae have increased dramatically over the last decades. Lipolysis is stimulated in the body mainly by the catecholamines adrenaline and noradrenaline which are elevated in the circulation, e.g., during fasting or exercise. Adrenaline and noradrenaline signal through both α- and β-adrenergic receptor and they thereby either decrease or increase, respectively, the intracellular levels of cyclic AMP (cAMP). An increased concentration of cAMP results in the activation of adipose triacylglycerol lipase (ATGL) and hormone sensitive lipase (HSL), the two rate-limiting lipases responsible for lipolysis. Insulin counteracts the stimulation of lipolysis in adipocytes by activation of phosphodiesterase 3B (PDE3B) that degrades cAMP and thereby reduces the rate of lipolysis [1–3]. Lipolysis is thus under tight positive and negative hormonal control.

The signalling pathways involved in the control of lipolysis are highly complex, and numerous crosstalks between different pathways and branches are emerging. Jönsson *et al.* [3] provide detailed elucidation of the pathways controlling lipolysis in adipocytes from human subcutaneous adipose tissue and show a new β-adrenergic – insulin crosstalk, where β-adrenergic signalling, in addition to stimulation, also inhibits lipolysis via parts of the insulin signalling pathway. They also demonstrate an additional stimulatory lipolytic action of insulin at high concentrations of insulin. Beyond the actions mentioned in [3], Stich *et al.* also suggest an anti-lipolytic action of insulin involving α-adrenergic receptors [4]. This action was observed during microdialysis experiments, *in situ* in human subcutaneous adipose tissue, stimulated with adrenaline, isoproterenol, insulin and phentolamine. The high degree of crosstalk, and the different actions at different concentrations, make it hard to successfully grapple with all the data by mere reasoning. To understand the role and relative importance of these different actions of insulin in the control of lipolysis, a next step therefore is to test the suggested mechanisms in a formalized way using mathematical modelling.

We have earlier developed mathematical models for insulin signalling in human adipocytes in several steps, first in isolation and later connected to systemic glucose control models, and used the models to unravel key alterations in type 2 diabetes (T2D) [5–8]. These models have so far not included lipolysis and the control of lipolysis by insulin. We have also studied systemic whole-body effects of fatty acids on glucose uptake and release, using modelling [9], but with no link to intracellular lipolysis. There have also been other efforts to understand adipose tissue lipolysis in more detail systemically, for example experimentally in [10] and using mathematical modelling in [11, 12], but without detailed intracellular components. In summary, none of the existing models have been developed to unravel the mechanisms of control of intracellular lipolysis.

Here, we develop a new model for lipolysis and the release of fatty acids based on both *in vitro* and *in vivo* experimental data from humans (Fig. 1). The model includes all three suggested insulin actions on lipolysis: two actions via the insulin receptor directly, one anti-lipolytic and one lipolytic, and a third indirect anti-lipolytic action via the α-adrenergic receptors. Using mechanistic modelling, we can evaluate the impact of these actions individually. The model accurately predicts new independent

validation data and is therefore useful to simulate new *in silico* experiments, such as the release of fatty acids *in vivo*, under both non-diabetic and type 2 diabetic conditions. The developed model is the first multilevel model for the hormonal control of lipolysis, and it opens for new research and drug discovery related to type 2 diabetes.

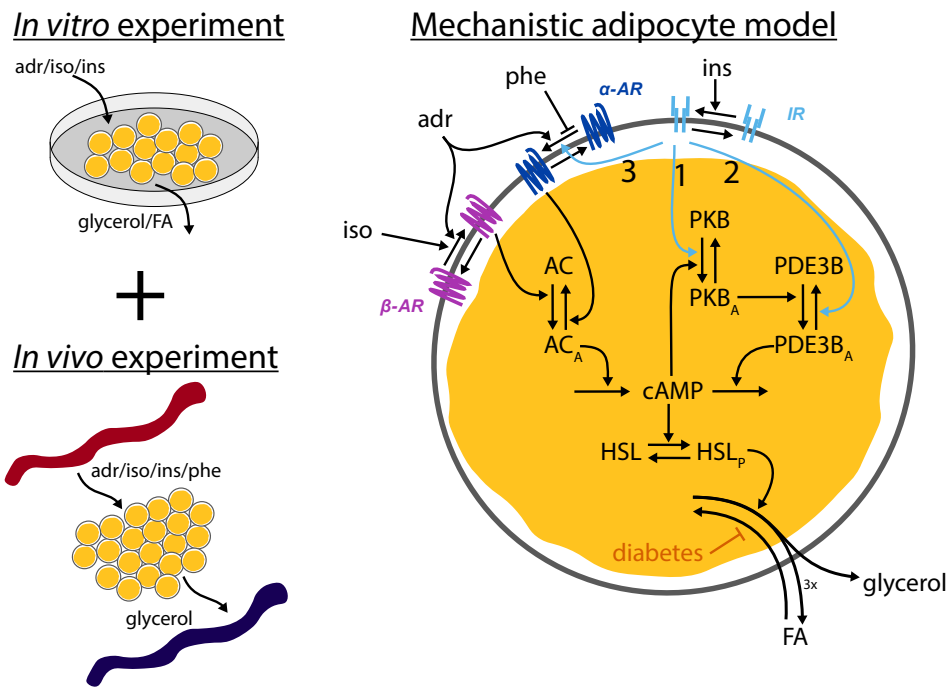

Figure 1: The system under study. Data from both *in vitro* and *in vivo* experiments of stimulated lipolysis using insulin, adrenergic stimulus, and phentolamine were combined to create a first multilevel mechanistic model of lipolysis, under both non-diabetic and type 2 diabetic conditions. The model responds to stimulus with adrenaline (adr), isoproterenol (iso), insulin (ins), and phentolamine (phe), initiating signalling cascades through key proteins leading to release of fatty acids (FA) and glycerol. Adr affects both β-adrenergic receptors (β-AR) and α-adrenergic receptors (αAR), while iso only affects βAR. Ins affects the insulin receptor (IR), leading to three different insulin actions: 1) an anti-lipolytic effect of insulin via protein kinase B (PKB) and phosphodiesterase 3B (PDE3B), 2) a positive lipolytic effect via PDE3B at high insulin concentrations, and 3) an anti-lipolytic effect of insulin via α-adrenergic receptors.

Results

To connect data from several sources into a common framework, we use mechanistic modelling. In mechanistic modelling, available knowledge about a system is formulated as a model by constructing a set of ordinary differential equations. The validity of such models can be tested by comparing model simulations to experimental data. Typically, the values of the model parameters, e.g. kinetic rate constants and initial concentrations of substances, are unknown and need to be estimated by training the model to experimental data. Other experimental data are then used for testing and validating the predictive power of the model.

Experimental observations and model development

We aimed to develop a mechanistic model focused on the regulation of intracellular lipolysis and the release of fatty acids and glycerol from the adipose tissue. The model is based on data from both *in vitro* measurements on isolated adipocytes, and *in vivo* microdialysis measurements, in both cases from non-diabetic individuals. More specifically, to develop the model we used experimental data from two sources: i) isolated adipocytes treated *in vitro* with the β-adrenergic agonist isoproterenol to stimulate lipolysis, and additionally with insulin to inhibit the isoproterenol-stimulated lipolysis, from [3], and ii) microdialysis measurements of lipolysis *in vivo*, stimulated with adrenaline/isoproterenol and inhibited by insulin and phentolamine, from [4]. We have taken three previously suggested mechanisms of crosstalk for the actions of insulin to explain the observed behaviour in the data: 1) an anti-lipolytic effect of insulin via protein kinase B (PKB) and PDE3B [3, 13], 2) a positive lipolytic effect via PDE3B at high concentrations of insulin [3], and 3) an anti-lipolytic effect of insulin via α-adrenergic receptors [4]. We have also included other known signalling steps in the control of lipolysis in adipocytes as indicated in Fig. 1 and detailed in the Method section. To avoid overfitting, the model was kept "minimal" in the sense that we focused on a few key proteins, and not every protein known to be involved in the control of lipolysis.

Comparisons between model simulations and data

The model was trained to *in vitro* dose-response data for the phosphorylation of PKB and the release of glycerol and fatty acids in response to isoproterenol and insulin stimulation, as well as *in vivo* microdialysis data of glycerol release in response to adrenaline and insulin (Fig. 2; solid lines represent the model simulation with the best agreement to data, shaded areas represent the model uncertainty, and experimental data are represented as mean values with error bars (SEM)). The model uncertainty refers to the most extreme simulations, while still requiring the model to pass statistical tests. The best model simulation clearly has a good agreement with the experimental data (Fig. 2). This visual assessment is supported by a statistical χ^2-test, where the cost of the model (v^* for the optimal cost, see Materials and Methods), given the optimal parameter values, is below the threshold of rejection given by the χ^2-test ($v^* = 182 < \chi^2 - threshold = 198$) for a significance level of 0.05. The model uncertainty was estimated in the same way as in [14], by maximizing/minimizing the simulation in all experimental data points while requiring the cost to not exceed the χ^2-threshold for a significance level of 0.05.

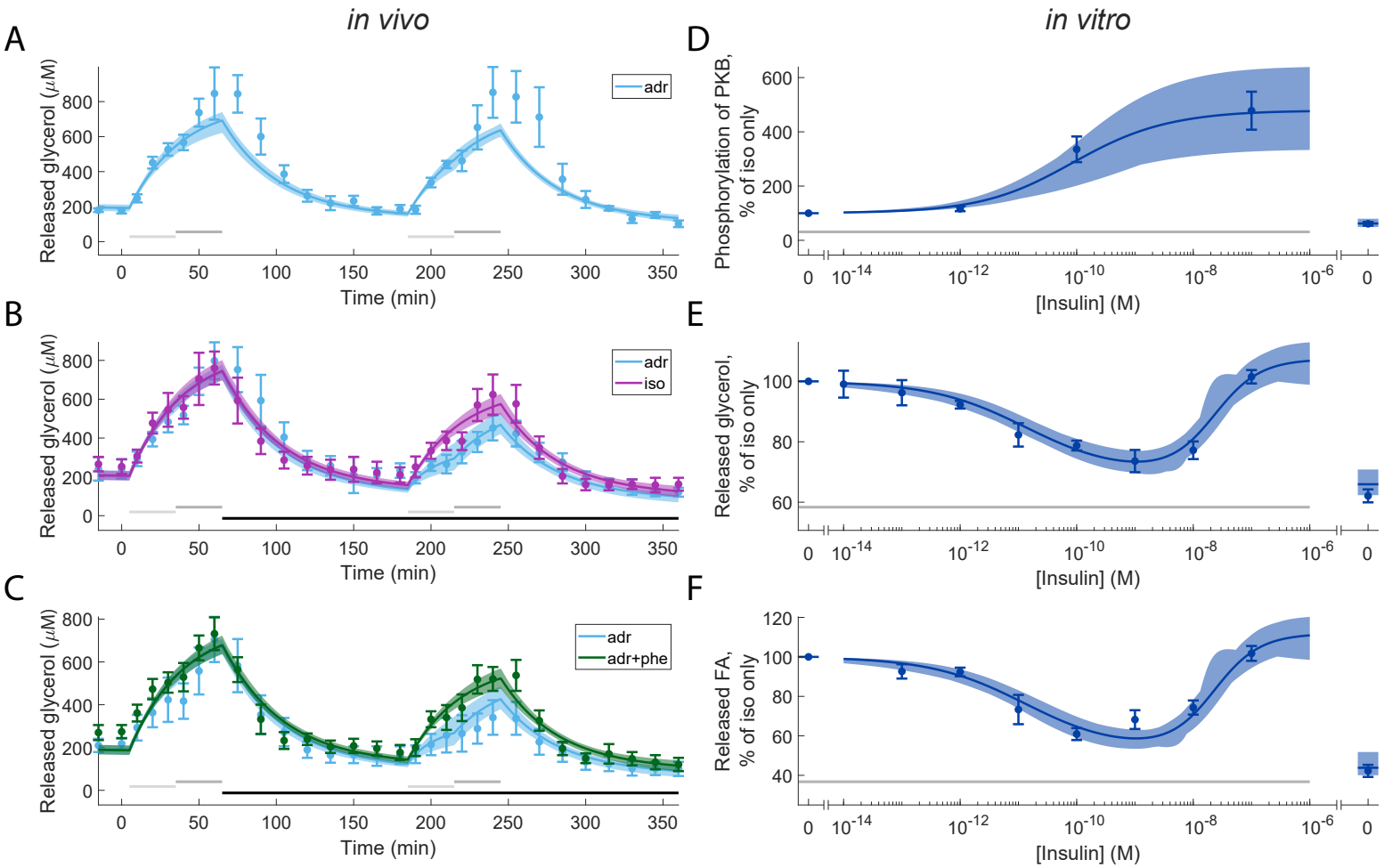

Figure 2: Estimation data and model simulations. In all panels, solid lines represent the model simulation with the best agreement to data, the shaded areas represent the model uncertainty, and experimental data points are represented as mean values with error bars (SEM). (A-C) are the *in vivo* time-series experiments, and (D-F) the *in vitro* dose-response experiments. In (A-C), horizontal light/dark grey lines represent stimulation with low/high adrenergic stimulus (1/10 μM adrenaline or 0.1/1 μM isoproterenol) with or without phentolamine (phe; 100 μM), horizontal black lines represent stimulation with insulin (0.6 nM) and in (D-F) horizontal grey lines represent simulation with isoproterenol (10 nM). In the *in vivo* experiments, experiments with adrenaline are shown in light blue (A-C), with isoproterenol in purple (B), and with the combined stimulation with adrenaline and phentolamine in green (C). In the *in vitro* experiments (D-F), increasing doses of insulin (x-axis) were given together with 10nM isoproterenol in all points except one. The point without isoproterenol got no stimulus and is shown to the right in the graphs. For full experimental details, see [4] for the *in vivo* experiments, and [3] for the *in vitro* experiments.

Model testing: predicting intracellular phosphorylation of HSL

For a model to be of practical use, it should be able to perform reasonable predictions. To test this, we used the model to predict the dose-response for phosphorylation of HSL (HSLp), an intracellular state in the model (Fig. 1) that was not used when training model to data. We estimated the uncertainty of the model prediction in the same way as described in the comparison between model and data, i.e. we maximized/minimized the prediction simulation, while requiring the agreement to the estimation data to be acceptable (cost below threshold, see **Statistical analysis** in Materials and methods). When

compared to the experimental data (Fig. 3), the model prediction appears to perform well. This was later confirmed with a χ^2-test, when the pool of available data was extended to include HSLp under non-diabetic conditions, and fatty acid release under diabetic conditions (see section **Estimating the extent of altered reesterification in type 2 diabetes** below).

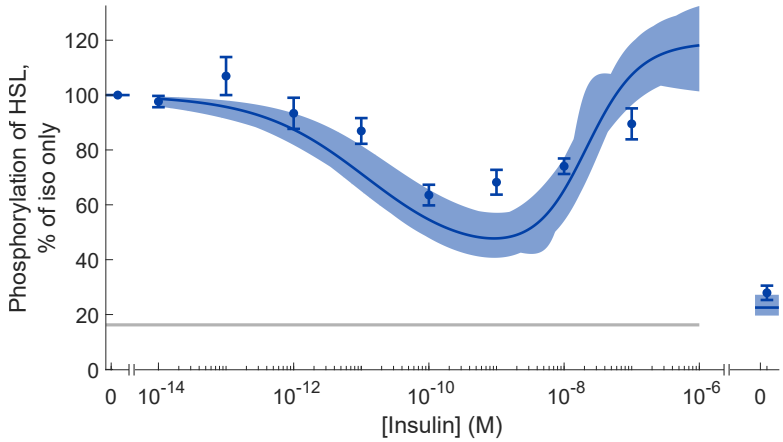

Figure 3: Prediction of intracellular levels of HSL phosphorylation. The solid line represents the model simulation with the best agreement to data, the shaded area represents the model uncertainty, and experimental data are represented as mean values with error bars (SEM). The horizontal grey line represent simulation with isoproterenol (10 nM). Increasing doses of insulin (x-axis) were given together with 10 nM isoproterenol in all points except one. The point without isoproterenol got no stimulus and is shown to the right in the graph. For the full experimental details, see [3].

Investigating the different actions of insulin

With the validated model, we continued to investigate the impact of the three different insulin actions (Fig. 1, the three blue arrows) by excluding one action at a time. We excluded an action by keeping the corresponding IR variable at basal levels throughout the simulation (instead of increasing with increased concentration of insulin) (Fig. 4). Firstly, by removing action 1) (the anti-lipolytic effect of insulin via PKB/PDE3B), the model is unable explain the decline in glycerol release in response to increased levels of insulin *in vitro*: compare Fig. 4A with Fig. 4C. Secondly, by removing action 2) (the positive lipolytic effect of insulin via PDE3B), the model is unable to explain the recovery in glycerol release at high insulin concentrations *in vitro*: compare Fig. 4A with Fig. 4E. And lastly, by removing action 3) (the anti-lipolytic effect of insulin via α-adrenergic receptors), the model is unable to explain the decrease in glycerol release in the second set of adrenergic stimuli *in vivo*: compare Fig. 4B with Fig. 4D. Consequently, all three actions of insulin are required to explain the available experimental data.

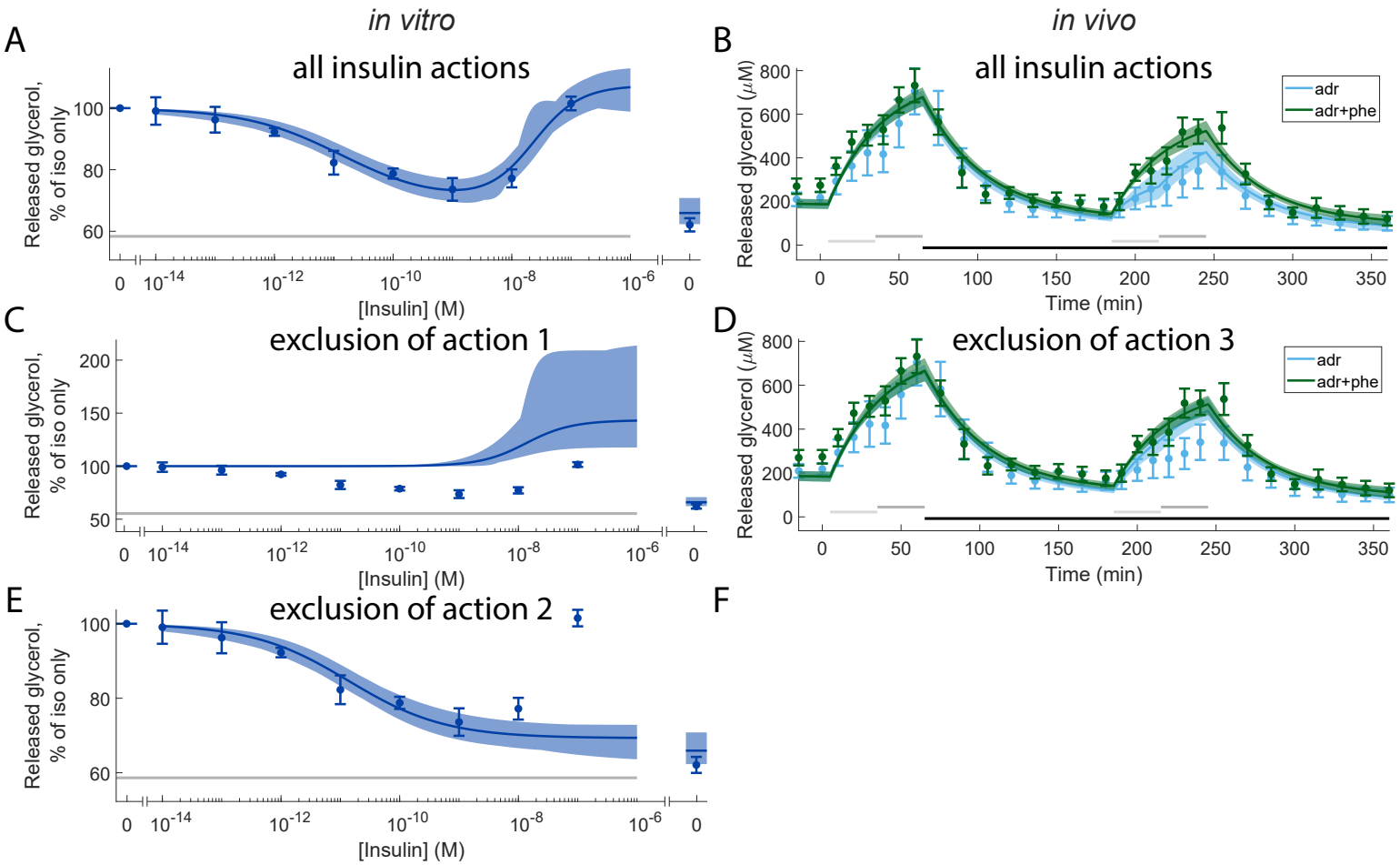

Figure 4: Effects of excluding either of the insulin actions. In panels (A-E), data points with error bars represent mean and SEM values, solid lines represent the model simulation with the best agreement to data, and the shaded areas represent the model uncertainty. (A, B) represent model simulations with all insulin actions present (same as Fig. 2C, F), see Fig. 1 for a graphical representation of the three insulin effects. (C-E) represent the model simulations when either of the actions are excluded. In (A, C, E) horizontal grey lines represent simulation with isoproterenol (10 nM) and in (B, D) horizontal light/dark grey lines represent stimulation with low/high dose of adrenalin (1/10 μM) with or without phentolamine (100 μM), horizontal black lines represent stimulation with insulin (0.6 nM). In the *in vitro* experiments (A, C, E), increasing doses of insulin (x-axis) were given together with 10nM isoproterenol in all points except one. The point without isoproterenol got no stimulus and is shown to the right in the graphs. In the *in vivo* experiments, experiments with adrenaline are shown in light blue (B, D) and with the combined stimulation with adrenaline and phentolamine in green (D).

Estimating the extent of altered reesterification in type 2 diabetes

We then used the validated model to gain new biological insights. As demonstrated in [3, Fig. 14D] at the cellular level, essentially only the release of fatty acids, but not of glycerol and hence not lipolysis, is affected in typ 2 diabetes. The authors conclude that this is due to reduced reesterification, i.e. a decreased reuse of fatty acids to re-form triacylglycerol, in the diabetic state. We used the model to quantify a range for the impairment of reesterification in type 2 diabetes. In order to estimate how much reesterification is altered in type 2 diabetes, we added a single parameter representing a decrease in reesterification with a range between 0 - 1. Furthermore, we extended the pool of data

to also include HSLp, the data previously used for validating the model. Beyond HSLp, we also included data for fatty acid release under diabetic conditions ([3, Fig. 14D]). We then trained the model, complemented with the reesterification impairment, to the extended pool of data, and used this retrained model to estimate the range of the impairment on the reesterification under diabetic conditions. The model uncertainty is shown for HSLp in Fig. 5A. Furthermore, the model uncertainty for the release of fatty acids under diabetic conditions is shown in Fig. 5B. The model uncertainty for the other measurables from Fig. 2 are shown in Fig. S1. As can be seen, the model agrees well with data, which is further supported by a χ^2-test ($v^* = 214 < \chi^2 - threshold = 218$). With the trained model, we found the range of impairment of the reesterification to be between 24 - 60% under diabetic conditions, which is in line with the results in [3] that demonstrate that the reesterification is reduced with 25% in type 2 diabetes.

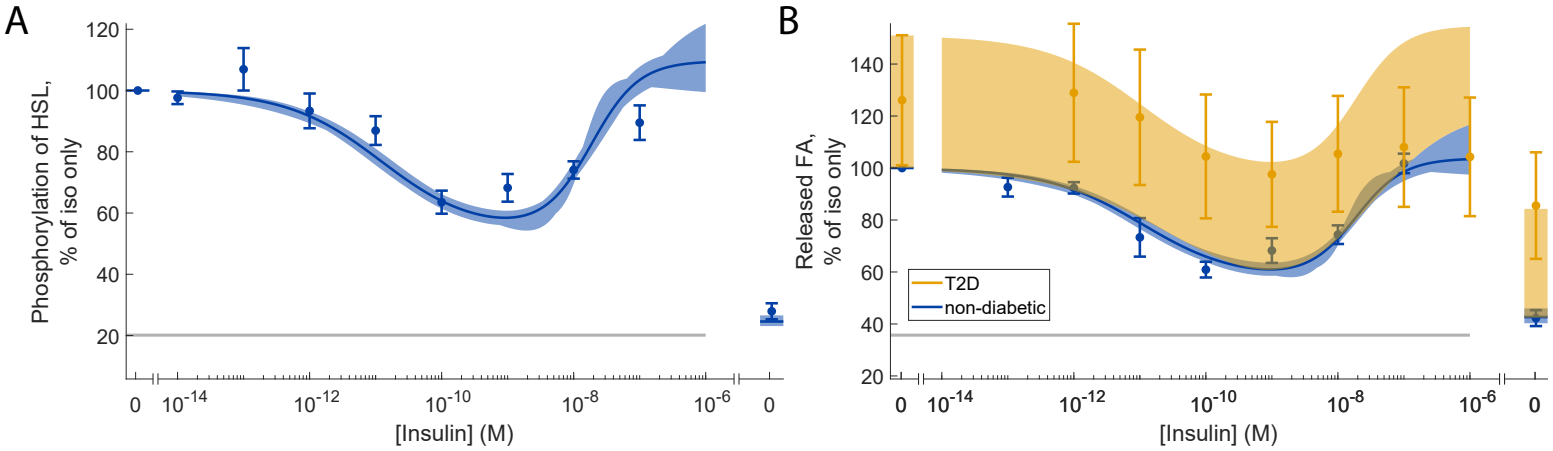

Figure 5: Model agreement when trained to the extended pool of data. In both panels, dots and error bars represents mean and SEM values, solid lines represent the model simulation with the best agreement to data, and the shaded areas represent the model uncertainty. Horizontal grey lines represent simulation with isoproterenol (10 nM). In both panels (A, B) increasing concentrations of insulin (x-axis) were given together with 10nM isoproterenol in all points except one. The point without isoproterenol got no stimulus and is shown to the right in the graphs. The experiments under non-diabetic conditions are shown in blue, and in (B) yellow represents the experiment under diabetic conditions. (A) shows the phosphorylation of HSL, and (B) shows the release of fatty acids (FA) under both under both non-diabetic and type 2 diabetic conditions. Note that the FA release under non-diabetic conditions is part of the original data, and is shown here to illustrate the difference between non-diabetic (blue) and type 2 diabetic (yellow) conditions. The agreement with the rest of the original dataset can be seen in Fig. S1. For the full experimental details, see [3].

In vivo model simulations of fatty acid release, under both non-diabetic and type 2 diabetic conditions

In addition to predicting dose-response data or quantifying the range of impairment on the reesterification of fatty acids, we can also use the model to predict temporal changes *in vivo*. As can be seen in Fig. 1, during lipolysis both glycerol and fatty acids are released from the adipocytes. However, only the time series for glycerol release were measured in the *in vivo* data used to train the model parameters. We can now use the model to not only predict the release of fatty acids *in vivo* in response to e.g. a treatment with adrenaline, we can also predict the fatty acid release *in vivo* under diabetic conditions. As expected, the release of fatty acids *in vivo* in response to adrenaline temporally mimics the release

of glycerol (Fig. 6). Furthermore, in line with the finding that the reesterification is impaired in the diabetic condition, resulting in a higher release of fatty acids from the adipocytes, the adipose tissue release of fatty acids *in vivo* are increased under diabetic conditions.

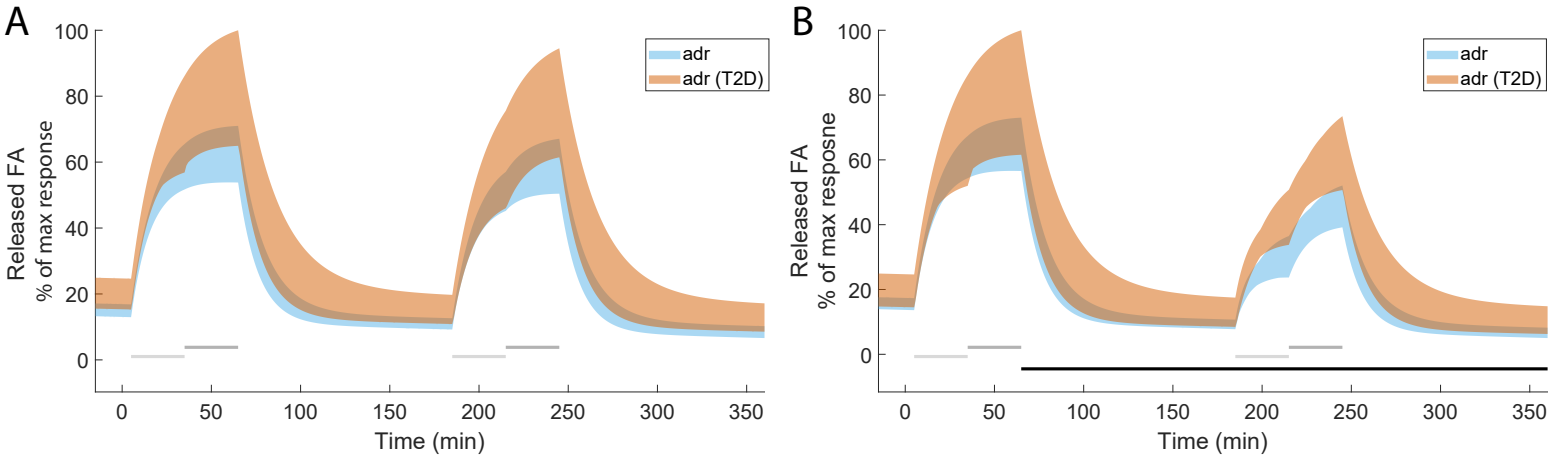

Figure 6: Simulations of fatty acid release *in vivo*, under both non-diabetic and type 2 diabetic conditions. In both panels, the shaded areas represent the model simulation uncertainty. In both panels, (A-B), horizontal light grey lines represent stimulation with 1 µM adrenaline, dark grey lines lines represent stimulation with 10 µM adrenaline, and horizontal black lines represent stimulation with 0.6 nM insulin. Light blue areas represent non-diabetic conditions, and orange areas represent type 2 diabetic conditions. (A) shows the model prediction without insulin, and (B) with insulin.

Materials and method

Data processing

In vitro experiments with isolated human adipocytes were performed by us and were previously published (Fig. 1 and 14D in [3]). *In vivo* data was extracted from Figs. 1A, 2A, and 3A in [4]. From the *in vitro* data, we removed one data point believed to be an outlier (the data point for ins = 10^{-14} M in the non-diabetic fatty acid release data). From the *in vivo* data, we removed all data related to a third peak (not shown), relating to events after the two peaks studied here, which are essentially repeats of the second peak, yet showing a different response. Details of these decisions are discussed in the Discussion section.

Mathematical modelling

A system of ordinary differential equations (ODEs) was used to model lipolysis and the release of fatty acids *in vitro* and *in vivo*. Here, we will now describe the model equations. The equations are also visualized in the interaction graph in Fig. 1. The full model with all described equations can be found in the supplementary files (see **Data and model availability**).

Equations for insulin actions

We modelled the three different actions of insulin described in [3, 4] (see Fig. 1) as three separate sigmoidal insulin receptor (IR) functions, all dependent on the concentration of insulin. These three

IR functions then affect downstream sites on PKB, PDE3B, and α-adrenergic receptor. The equation for these sigmoidal functions are described in Eq. (1).

$$IR_x = 100 + \frac{min_x - 100}{1 + (ins/EC50_x)^{n_x}}, \qquad x \in \{1,2,3\} \tag{1}$$

Here, IR_x is a function that is dependent on the given concentration of insulin (*ins*); min_x is the minimum value the function has at ins=0; $EC50_x$ is the concentration of insulin at which the function reaches half of the maximal response (which is set to 100). The steepness of the function is determined by n_x.

Equations for insulin signalling

When IR is stimulated with insulin, a signalling cascade is initiated which leads up to the activation of PKB, through insulin receptor substrate 1 (IRS1), phosphoinositide 3-kinase (PI3K), and Phosphoinositide-dependent kinase-1 (PDK1). In our model, we have simplified this cascade as a direct action from IR to the activation of PKB. PKB can also be activated by cAMP. We model PKB as either being in an inactive or an active configuration. The ODEs for PKB are given by Eq. (2)

$$\begin{aligned} d/dt(PKB) &= -(k1a \cdot cAMP + k1a2 \cdot IR_1) \cdot PKB + k1b \cdot PKBp \\ d/dt(PKBp) &= \quad (k1a \cdot cAMP + k1a2 \cdot IR_1) \cdot PKB - k1b \cdot PKBp \end{aligned} \tag{2}$$

Here, PKB and $PKBp$ are the two model states for the inactive and active form of PKB, IR_1 is the effect of insulin action 1, $cAMP$ is the levels of cAMP, and $k1a$ $k1a2$, and $k1b$ are rate determining parameters.

Downstream, PKB will directly activate PDE3B. Beyond the direct activation by PKB, PDE3B will also be inactivated by insulin action 2. The full mechanism for this activation is currently unknown. We model PDE3B as being in either an inactive or an active state. The ODEs for PDE3B are given in Eq. (3).

$$\begin{aligned} d/dt(PDE3B) &= -k2a \cdot PKBp \cdot PDE3B + k2b \cdot PDE3Ba \cdot IR_2 \\ d/dt(PDE3Ba) &= \quad k2a \cdot PKBp \cdot PDE3B - k2b \cdot PDE3Ba \cdot IR_2 \end{aligned} \tag{3}$$

Here, $PDE3B$ and $PDE3Ba$ are the two model states for the inactive and active form of PDE3B, $PKBp$ is the model state for activated PKB, IR_2 is the effect of insulin action 2, and $k2a$ and $k2b$ are rate determining parameters.

Equations for α-adrenergic receptor signalling

In the model, the α-adrenergic receptor can switch between two different configurations: activated or inactivated. This balance is offset towards the activated state when the α-adrenergic receptor is stimulated with adrenaline. The activated receptor will passively return to the inactive configuration. The activation of the α-adrenergic receptor is also augmented by insulin and inhibited by the addition of phentolamine. The ODEs for the α-adrenergic receptor are given in Eq. (4).

$$\begin{aligned} d/dt(ALPHA) &= -(k3a \cdot IR_3) \cdot adr \cdot (1 - phe) \cdot ALPHA + k3b \cdot ALPHAa \\ d/dt(ALPHAa) &= \quad (k3a \cdot IR_3) \cdot adr \cdot (1 - phe) \cdot ALPHA - k3b \cdot ALPHAa \end{aligned} \tag{4}$$

Here, $ALPHA$ and $ALPHAa$ are the two model states for the inactive and active α-adrenergic receptor,

adr and phe are the stimulation given as inputs, IR_3 is insulin action 3, and $k3a$ and $k3b$ are rate determining parameters. Note that the receptor activation is turned off when $phe = 1$.

Equations for β-adrenergic receptor signalling

The β-adrenergic receptor, similarly to the α-adrenergic receptor, is also switching between two configurations. In contrast to the α-adrenergic receptor, the β-adrenergic receptor is also activated by adrenalin. Due to the uncertainty in difference in activation between adrenaline and isoproterenol, we added a scaling factor on isoproterenol. Furthermore, the activation of the β-adrenergic receptor is not increased by insulin or inhibited by phentolamine. The ODEs for the β-adrenergic receptor are given in Eq. (5).

$$\begin{aligned} d/dt(BETA) &= -(k4a \cdot (iso \cdot isoscale + adr) + k4a2) \cdot BETA + k4b \cdot BETAa \\ d/dt(BETAa) &= \quad (k4a \cdot (iso \cdot isoscale + adr) + k4a2) \cdot BETA - k4b \cdot BETAa \end{aligned} \tag{5}$$

Here, $BETA$ and $BETAa$ are the two model states for the inactive and active β-adrenergic receptor, adr and iso are inputs corresponding to stimulation with adrenaline and isoproterenol, and $k4a$, $isoscale$, $k4a2$, and $k4b$ are rate determining parameters.

Equations for lipolysis

Both the β-adrenergic receptor and the α-adrenergic receptor are G-protein coupled receptors. The G-proteins is made of multiple subunits, which will disassociate when the receptors are activated. These subunits will then go on and trigger another downstream effector. One such effector is adenylyl cyclase, which catalyse the conversion of ATP into cAMP. Through the G-proteins, β-adrenergic receptor will increase the activity of adenylyl cyclase, and α-adrenergic receptor will decrease the activity. In the model, we have simplified this interaction by ignoring the G-proteins, letting the β-adrenergic receptor and α-adrenergic receptor directly affect the adenylyl cyclase. Furthermore, we model the adenylyl cyclase as being either inactive or active, where the active version leads to an increased production of cAMP. The model equations are given in Eq. (6).

$$\begin{aligned} d/dt(AC) &= -k5a \cdot (BETAa) \cdot AC + k5b \cdot (ALPHAa) \cdot ACa \\ d/dt(ACa) &= \quad k5a \cdot (BETAa) \cdot AC - k5b \cdot (ALPHAa) \cdot ACa \end{aligned} \tag{6}$$

Here, AC and ACa are the two model states for inactive and active adenylyl cyclase respectively, $BETAa$ and $ALPHAa$ are the model states for active β- and α-receptor, and $k5a$ and $k5b$ are rate determining parameters.

Downstream of both adenylyl cyclase and PDE3B is cAMP. An increase in adenylyl cyclase activation will lead to an increased concentration of cAMP, and an increase in PDE3B activation will lead to a decreased concentration of cAMP. Together, adenylyl cyclase and PDE3B balance the concentration of cAMP in the cell. cAMP have negative feedback loop by activating PKB via PI3K, which in turn activates PDE3B, which leads to a decreased concentration of cAMP. We have also added both a basal production and degradation of cAMP. The ODEs for cAMP are given in Eq. (7).

$$d/dt(cAMP) = k6basal + k6a \cdot ACa - (k6b \cdot PDE3Ba + k6b2) \cdot cAMP \tag{7}$$

Here, $cAMP$ is the model state for cAMP, ACa and $PDE3Ba$ are the model states for the active configurations of adenylyl cyclase and PDE3B, and $k6basal$, $k6a$, $k6b$, and $k6b2$ are rate determining

parameters.

The concentration of cAMP indirectly controls the lipolysis by activation of protein kinase A (PKA), which in turn will activate the lipid droplet-coating protein perilipin 1 (PLIN1) and hormone-sensitive lipase (HSL). Activation of PKA leads to the phosphorylation of the lipid droplet-coating protein perilipin 1 (PLIN1) and its subsequent release of the adipose triacylglycerol lipase (ATGL) activator, comparative gene identification-58. Active ATGL will catalyse the hydrolysis of the first fatty acid of the triacylglycerol. Phosphorylation of HSL by PKA results in activation and translocation of HSL to the lipid droplet, where HSL hydrolyses the second fatty acid leaving monoacylglycerol to be hydrolysed by a constitutively active monoacylglycerol lipase. HSL is capable to hydrolyse triacylglycerol, but ATGL is believed to be more important in this rate-limiting step of lipolysis. In the model, we simplified these interactions by only modelling HSL with an input from cAMP. The ODEs are given in Eq. (8).

$$\begin{aligned} d/dt(HSL) &= -k7a \cdot cAMP \cdot HSL + k7b \cdot HSLp \\ d/dt(HSLp) &= \quad k7a \cdot cAMP \cdot HSL - k7b \cdot HSLp \end{aligned} \tag{8}$$

Here, HSL and $HSLp$ are the states for inactive and active HSL, $cAMP$ is the model state for cAMP, and $k7a$ and $k7b$ are the rate determining parameters.

Once the triacylglycerol has been broken down into three fatty acids and one glycerol, the glycerol will be transported out of the cell, and the fatty acids will either be transported out or reesterified with glycerol-3P into new triacylglycerol. This reesterification is reduced in type 2 diabetes. Some of the fatty acids can also go back into the cell, while the glycerol cannot. Fatty acids and glycerol outside of the cell will be cleared in an *in vivo* setting, but not *in vitro*. The ODEs are given in Eq. (9).

$$\begin{aligned} d/dt(Gly) &= \quad k8a \cdot HSLp - k8b \cdot Gly \\ d/dt(FFA) &= 3 \cdot k8a \cdot HSLp - (k8b + k8c \cdot diab) \cdot FFA \end{aligned} \tag{9}$$

Here, Gly and FFA are the states for glycerol and fatty acids, $HSLp$ is the state for activated HSL, $diab$ is a parameter controlling the reduction of reesterification under diabetic conditions, and $k8a$, $k8b$, and $k8c$ are rate determining parameters. $k8a$ corresponds to the transport of fatty acids and glycerol from the inside to the outside of cell, $k8b$ is the clearance of fatty acids and glycerol *in vivo* (clearance was disabled *in vitro* by setting $k8b = 0$), and $k8c$ is the reesterification of fatty acids into triacylglycerol. To simulate the effect of type 2 diabetes on the reesterification, the parameter $diab$ was allowed to vary between 0.0 – 1.0. In non-diabetic conditions, the type 2 diabetes effect was disabled by setting $diab = 1$ (i.e. no effect of type 2 diabetes).

Experimental parameters

In the *in vivo* experiments, we introduced a linear drift parameter as well as a scaling constant. The scaling constant was calculated using MATLABs least squares with known covariance (lscov) function. In essence, the measurement equation can be expressed as in Eq. (10), exemplified for glycerol.

$$\hat{y}_{Gly} = k_{scale} \cdot (Gly - k_{drift} \cdot time) \tag{10}$$

Here, Gly and $\hat{y}_{Gly}$ are the model state and measurement equation for glycerol, k_{scale} is the scaling constant, $k_{drift} \cdot time$ is the offset due to the drift over time.

Initial values
All initial values of the ODEs were set to arbitrary non-negative values:

$$BETA(0) = 80,\ BETAa(0) = 5,\ ALPHA(0) = 80,\ ALPHAa(0) = 20,\ AC(0) = 75,\ ACa(0) = 25,$$
$$PKB(0) = 20,\ PKBp(0) = 80,\ PDE3B(0) = 20,\ PDE3Ba(0) = 80,\ cAMP(0) = 1,\ HSL(0) = 85,$$
$$HSLp(0) = 15,\ Gly(0) = 220,\ FFA(0) = 0$$

Quantifying the model agreement to experimental data
In order to evaluate the model's performance, we quantified the model agreement to data using a function typically referred to as a cost function. In this case, we used the normalized sum of squared residual as cost function (Eq. (11)).

$$v(\theta) = \sum_t \left(\frac{y_t - \hat{y}_t(\theta)}{SEM_t} \right)^2 \tag{11}$$

Here, $v(\theta)$ is the cost, equal to the sum of the normalized residual over all measured time points, t; p is the parameters; y_t is the measured data and $\hat{y}_t(\theta)$ is the model simulations; SEM_t is the standard error of the mean for the measured data.

Statistical analysis
To reject models, we used the χ^2-test with a significance level of 0.05. We used 167 degrees of freedom for the original training data (171 data points, minus 4 scaling parameters) leading to a threshold for rejection of $\chi^2(0.05, 167) \approx 198$. For the extended pool of data, used in the section **Investigating the different actions of insulin** in the results (including the release of fatty acids under diabetic conditions and HSLp), we used 185 degrees of freedom, resulting in a threshold for rejection of $\chi^2(0.05, 185) \approx 218$. Any combination of model and parameter set that results in a cost (Eq. (11)) above the threshold have to be rejected. If no parameter set exists for a model that results in a sufficiently low cost, the model structure has to be rejected.

Uncertainty estimation
The uncertainty of the model simulations for estimation, validation, and predictions, were gathered as proposed in [15] and implemented in [14]. Briefly, the model simulation for a single combination of experiment and time point was either maximized or minimized, while requiring the cost (Eq. (11)) to be below the χ^2-threshold. Compared to traditional profile-likelihood analysis (Eq. (12)),

$$\begin{aligned} \text{minimize} \quad & v(\theta) \\ \text{subject to} \quad & \hat{p} = \hat{y}_t(\theta), \\ & \hat{p} = p. \end{aligned} \tag{12}$$

where the prediction is stepped through to find the boundaries, we instead inverse the problem and solve it directly (Eq. (13)).

$$\text{minimize} \quad \hat{p} \tag{13a}$$

$$\text{subject to} \quad \hat{p} = \hat{y}_t(\theta), \tag{13b}$$

$$v(\theta) \leq \chi^2. \tag{13c}$$

In practice, the constraint (Eq. (13c)) is relaxed into the objective function as a L1 penalty term with an arbitrary offset if $V(\theta) > \chi^2$. We solved the maximization problem as a minimization problem, by changing sign of the prediction ($-\hat{p}$)

Optimization and software

We used MATLAB R2020a (MathWorks, Natick, MA) and the IQM toolbox (IntiQuan GmbH, Basel, Switzerland), a continuation of [16], for modelling. The parameter values were estimated using the enhanced scatter search (eSS) algorithm from the MEIGO toolbox [17]. eSS were restarted multiple times, partially run in parallel at the local node of the Swedish national supercomputing centre (NSC). We allowed the parameter estimation to freely find the best possible combinations of parameter values, within boundaries. The bounds of the parameter values are given in supplementary Table S1.

Discussion

The worldwide increase in obesity and type 2 diabetes highlights the importance of understanding how the adipose tissue, a central player of the whole-body energy homeostasis, store and release energy in the form of fat. We studied these processes, both during non-diabetic physiological conditions and when disturbed e.g. due to overeating, insulin resistance, or type 2 diabetes.

We here present a mathematical model of hormonal control of lipolysis in human adipose tissue (Fig. 1), a multi-level model that links molecular events at the cellular level with corresponding responses at the tissue level. The model can explain both *in vivo* temporal data from microdialysis experiments in adipose tissue (Fig. 2A-C and Fig. S1A-C) and *in vitro* dose-response data from isolated adipocytes (Fig. 2D-F, Fig. 5, and Fig. S1D-F), as well as accurately predict independent validation data (Fig. 3).

There exist other models of lipolysis in humans. For example [18] modelled insulin levels and fatty acid release in response to glucose intake on a systemic level, but do not model any adrenergic stimulus or have a detailed intracellular compartment. A more extensive model of lipid metabolism [12], is also missing a detailed intracellular compartment and adrenergic stimulus. Conversely, [19] modelled lipolysis in response to adrenergic stimulus with a detailed intracellular compartment, but lacked insulin signalling. Tangentially, there also exist models of glucose homeostasis with insulin signalling, but lacking both lipolysis and adrenergic hormonal control [7,20]. The model of hormonal control of lipolysis presented here is the first, to our knowledge, that includes insulin and adrenergic signalling, as well as an intracellular compartment. Some of the existing models are more detailed for certain aspects of lipolysis. We have chosen to only include sub-systems directly supported by included data, and the presented model can therefore be considered ”minimal”.

The presented model is in agreement with the experimental data, as visualized in Figs. 2, 5 and S1 (cf. the optimal parameter set in solid lines and the data). Furthermore, the estimated uncertainty of the model is reasonably large compared to the data uncertainty (cf. the shaded area and the error bars). This means that we probably have been successful in the collection of values of parameters. An interesting aspect of the cellular estimation data, which is also captured by the model, is that for high concentrations of insulin, lipolysis is stimulated even slightly beyond the isoproterenol-stimulated level (Fig. 2E-F). In the model, this behaviour originates from insulin action 2 (Fig. 1), as can be seen when insulin action 1 and 2, respectively, are removed (Fig. 4C,E). Insulin action 3 – anti-lipolytic effect of insulin via α-adrenergic receptors – was needed to explain the combined effect of adrenaline, insulin, and phentolamine in the *in vivo* estimation data [4], as shown when removed (second peak in Fig. 4D). It should be noted that insulin action 3, via the α-receptor, is also only observed at high concentrations of insulin, and may therefore be a secondary effect elicited by insulin in other cells or tissues.

Beyond investigating the contributions of the different insulin actions, we used the model to quantify the range of impairment on the reesterification in type 2 diabetes, which was reduced 24 - 60 %. Due to the large uncertainty in the data for the diabetic condition (Fig. 5B), the range is also uncertain. This predicted interval can be related to an estimated reduced reesterification of around 20 - 35 % in type 2 diabetes based on the same data without the use of modelling [3]. We also used the model to predict the temporal release of fatty acids *in vivo* in response to adrenaline in both non-diabetic and type 2 diabetic conditions (Fig. 6). Type 2 diabetes and obesity have traditionally been associated with elevated levels of circulating fatty acids, an issue both challenged and affirmed lately [10, 21]. Our model predicts an *in vivo* increase in the release of fatty acids in diabetic conditions versus in non-diabetic conditions. However, our model does not include mechanisms for fatty acid clearance due to uptake by other organs and therefore cannot predict the systemic levels of fatty acids or potential changes to the clearance in type 2 diabetes.

We used data from two different sources [3, 4] to develop the model, which can be seen both as a strength and as a weakness. Internally consistent data, from the same laboratory under the same experimental conditions, is potentially important to be able to test hypotheses to unravel new biological mechanisms. For the purpose herein, to develop a first intracellular model of lipolysis that includes key observations and that later can be further built upon, when more data become available, we believe it is a strength to use data from multiple sources. This means that the model is more general, and therefore more likely to be useful together with other human data from studies of adipose tissue lipolysis.

Desensitization, i.e. that cells decrease their response to stimuli with time, is a known phenomenon of β-adrenergic signalling. Stich et al [4] controlled for desensitization by using multiple repeats of the stimulus paradigm. We decided to only include the first two rounds of stimulation of lipolysis, as we think there is a tendency to desensitization in the third stimulation, and we decided not to include this behaviour in this first model. There are other studies that show a clear desensitization in the release of glycerol in response to adrenaline [22, 23]. These studies have shorter intervals between stimuli (30 min, 1 h), and also reveal desensitization due to exercise-induced stimulation of lipolysis [23]. We have previously studied desensitization in heart cells using modelling and found that dose-response curves need to be adjusted for this phenomenon before important parameters such as the EC50a are computed [24]. Desensitization is an important phenomenon in β-adrenergic signalling that should

not be overlooked and should be included in later models of lipolytic control.

In addition to excluding the third peak in the *in vivo* data, as discussed above, we also excluded the data point for the lowest concentration of insulin in the data on fatty acid release from the *in vitro* data. In that point, the response was significantly lower than either the point with no insulin or in response to the slightly higher concentration of insulin. We do not find that behaviour reasonable, and argue that that data point is an outlier.

During the modelling, we constrained insulin action 2 (Fig. 1) so that the EC50 in response to insulin stayed between 0.5 and 1.1 nM. The reasoning behind this constraint is that known upstream signalling intermediaries, such as the autophosphorylation of the insulin receptor, has an EC50 in that range [5]. We also included a slightly delayed response to changes in adrenaline and isoproterenol stimulus *in vivo* when developing the model. Such a delay was observed in the microdialysis data [4], but not as obviously present in primary adipocytes [3]. In effect, we delayed the time for all changes of adrenaline and isoproterenol concentrations with 5 min when simulating the *in vivo* data (e.g. in Fig. 2A-C). The agreement between model simulations and data became substantially better with this delay. The underlying cause behind the observed delay in the microdialysis setup could be pooling of data or a delay in the microdialysis probe – or a biological tissue effect. We have chosen not to include the mechanisms of the delay in the model, instead we explicitly added the time delay.

The model developed herein can be further developed in several directions. First, on the intracellular side, we aim to combine the model with our extensive work on the modelling of insulin signalling pathways in both non-diabetic and type 2 diabetic conditions [5–8]. With such a connection, we will reach a first model for the human adipocyte that is based on extensive data from both non-diabetic and type 2 diabetic patients. Such a model would be able to simulate the major functions of the adipocyte: the control of lipolysis, as well as insulin control of glucose uptake, protein synthesis, and transcription. Second, on the systemic regulation of fatty acid release, the work herein opens up for a first connected model where intracellular components of lipolysis are connected to whole-body changes in fatty acid release. This connected model can also be combined with other models, for example models for intake of meals. Such a connected model is key to understand mechanisms of ectopic fat storage, i.e. where liver and muscle tissue increase their storage of lipids – a condition that is linked to disease development such as in type 2 diabetes, liver failure, and cardiovascular disease [25].

Data and model availability

The experimental data as well as the complete code for data analysis and modelling are available at `https://github.com/willov/lipolysis` (DOI: 10.5281/zenodo.4327563) and is mirrored at `https://gitlab.liu.se/ISBgroup/projects/lipolysis`.

Author Contributions: All authors were involved in the writing of the paper. EN designed the study. WL, JE, and EN performed the modelling, All authors analysed data.

Conflict of interest: The authors declare that they have no conflict of interest.

Funding information: PS acknowledges support from Linköping University, the Swedish Diabetes Fund (a 3-years program), and the Swedish Research Council (a 5-years program). EN acknowledges support from the Swedish Research Council (Dnr 2019-03767), the Heart and Lung Found-

ation, and CENIIT (20.08). GC acknowledges support from the Swedish Research Council(Dnr 2018-05418, 2018-03319), Swedish Foundation for Strategic Research (ITM17-0245), SciLifeLab and KAW (2020.0182), Horizon 2020 (PRECISE4Q, 777107), CENIIT (15.09), ELLIIT, and the Swedish Fund for Research without Animal Experiments.

References

[1] Eriksson H, Ridderstråle M, Degerman E, Ekholm D, Smith CJ, Manganiello VC, et al. Evidence for the key role of the adipocyte cGMP-inhibited cAMP phosphodiesterase in the antilipolytic action of insulin. BBA - Molecular Cell Research. 1995 apr;1266(1):101–107.

[2] Schmitz-Peiffer C, Reeves ML, Denton RM. Characterization of the cyclic nucleotide phosphodiesterase isoenzymes present in rat epididymal fat cells. Cellular Signalling. 1992 jan;4(1):37–49.

[3] Jönsson C, Batista APC, Kjølhede P, Strålfors P. Insulin and β-adrenergic receptors mediate lipolytic and anti-lipolytic signalling that is not altered by type 2 diabetes in human adipocytes. Biochemical Journal. 2019 oct;476(19):2883–2908.

[4] Stich V, Pelikanova T, Wohl P, Sengenès C, Zakaroff-Girard A, Lafontan M, et al. Activation of α2-adrenergic receptors blunts epinephrine-induced lipolysis in subcutaneous adipose tissue during a hyperinsulinemic euglycemic clamp in men. American Journal of Physiology-Endocrinology and Metabolism. 2003 sep;285(3):E599–E607.

[5] Brännmark C, Nyman E, Fagerholm S, Bergenholm L, Ekstrand EM, Cedersund G, et al. Insulin signaling in type 2 diabetes: experimental and modeling analyses reveal mechanisms of insulin resistance in human adipocytes. The Journal of biological chemistry. 2013 apr;288(14):9867–80.

[6] Nyman E, Rajan MR, Fagerholm S, Brännmark C, Cedersund G, Strålfors P. A single mechanism can explain network-wide insulin resistance in adipocytes from obese patients with type 2 diabetes. Journal of Biological Chemistry. 2014;289(48).

[7] Rajan MR, Nyman E, Kjølhede P, Cedersund G, Strålfors P. Systems-wide experimental and modeling analysis of insulin signaling through forkhead box protein O1 (FOXO1) in human adipocytes, normally and in type 2 diabetes. Journal of Biological Chemistry. 2016;291(30).

[8] Nyman E, Brännmark C, Palmér R, Brugård J, Nyström FH, Strålfors P, et al. A hierarchical whole-body modeling approach elucidates the link between in vitro insulin signaling and in vivo glucose homeostasis. Journal of Biological Chemistry. 2011 jul;286(29):26028–26041.

[9] Sips FLP, Nyman E, Adiels M, Hilbers PAJ, Strålfors P, Van Riel NAW, et al. Model-based quantification of the systemic interplay between glucose and fatty acids in the postprandial state. PLoS ONE. 2015 sep;10(9).

[10] Karpe F, Dickmann JR, Frayn KN. Fatty Acids, Obesity, and Insulin Resistance: Time for a Reevaluation. Diabetes. 2011 Oct;60(10):2441–2449. Publisher: American Diabetes Association Section: Perspectives in Diabetes.

[11] O'Donovan SD, Lenz M, Vink RG, Roumans NJT, De Kok TMCM, Mariman ECM, et al. A computational model of postprandial adipose tissue lipid metabolism derived using human arteriovenous stable isotope tracer data. PLoS Computational Biology. 2019;15(10):e1007400.

[12] Pratt AC, Wattis JAD, Salter AM. Mathematical modelling of hepatic lipid metabolism. Mathematical Biosciences. 2015 Apr;262:167–181.

[13] Degerman E, Ahmad F, Chung YW, Guirguis E, Omar B, Stenson L, et al.. From PDE3B to the regulation of energy homeostasis. Elsevier Ltd; 2011.

[14] Lövfors W, Simonsson C, Komai AM, Nyman E, Olofsson CS, Cedersund G. A systems biology analysis of adrenergically stimulated adiponectin exocytosis in white adipocytes. bioRxiv. 2020.

[15] Cedersund G. Conclusions via unique predictions obtained despite unidentifiability - new definitions and a general method. FEBS Journal. 2012 sep;279(18):3513–3527.

[16] Schmidt H, Jirstrand M. Systems Biology Toolbox for MATLAB: a computational platform for research in systems biology. Bioinformatics. 2006 Feb;22(4):514–515. Publisher: Oxford Academic.

[17] Egea JA, Henriques D, Cokelaer T, Villaverde AF, MacNamara A, Danciu DP, et al. MEIGO: an open-source software suite based on metaheuristics for global optimization in systems biology and bioinformatics. BMC Bioinformatics. 2014 May;15(1):136.

[18] L Murillo A, Li J, Castillo-Chavez C. Modeling the dynamics of glucose, insulin, and free fatty acids with time delay: The impact of bariatric surgery on type 2 diabetes mellitus. Mathematical Biosciences and Engineering. 2019;16(5):5765–5787.

[19] Kim J, Saidel GM, Kalhan SC. A computational model of adipose tissue metabolism: Evidence for intracellular compartmentation and differential activation of lipases. Journal of theoretical biology. 2008 Apr;251(3):523–540.

[20] Smith JMD, Maas JA, Garnsworthy PC, Owen MR, Coombes S, Pillay TS, et al. Mathematical modeling of glucose homeostasis and its relationship with energy balance and body fat. Obesity (Silver Spring, Md). 2009 Apr;17(4):632–639.

[21] Arner P, Rydén M. Fatty Acids, Obesity and Insulin Resistance. Obesity Facts. 2015;8(2):147–155. Publisher: Karger Publishers.

[22] Stallknecht B, Bülow J, Frandsen E, Galbo H. Desensitization of human adipose tissue to adrenaline stimulation studied by microdialysis. Journal of Physiology. 1997 apr;500(1):271–282.

[23] Marion-Latard F, De Glisezinski I, Crampes F, Berlan M, Galitzky J, Suljkovicova H, et al. A single bout of exercise induces β-adrenergic desensitization in human adipose tissue. American Journal of Physiology - Regulatory Integrative and Comparative Physiology. 2001 jan;280(1 49-1).

[24] Nyman E, Lindgren I, Lövfors W, Lundengård K, Cervin I, Sjöström TA, et al. Mathematical modeling improves EC50 estimations from classical dose-response curves. FEBS J. 2015 feb.

[25] Heilbronn L, Smith SR, Ravussin E. Failure of fat cell proliferation, mitochondrial function and fat oxidation results in ectopic fat storage, insulin resistance and type II diabetes mellitus. International Journal of Obesity. 2004 Dec;28(4):S12–S21. Number: 4 Publisher: Nature Publishing Group.

Supplemental Material

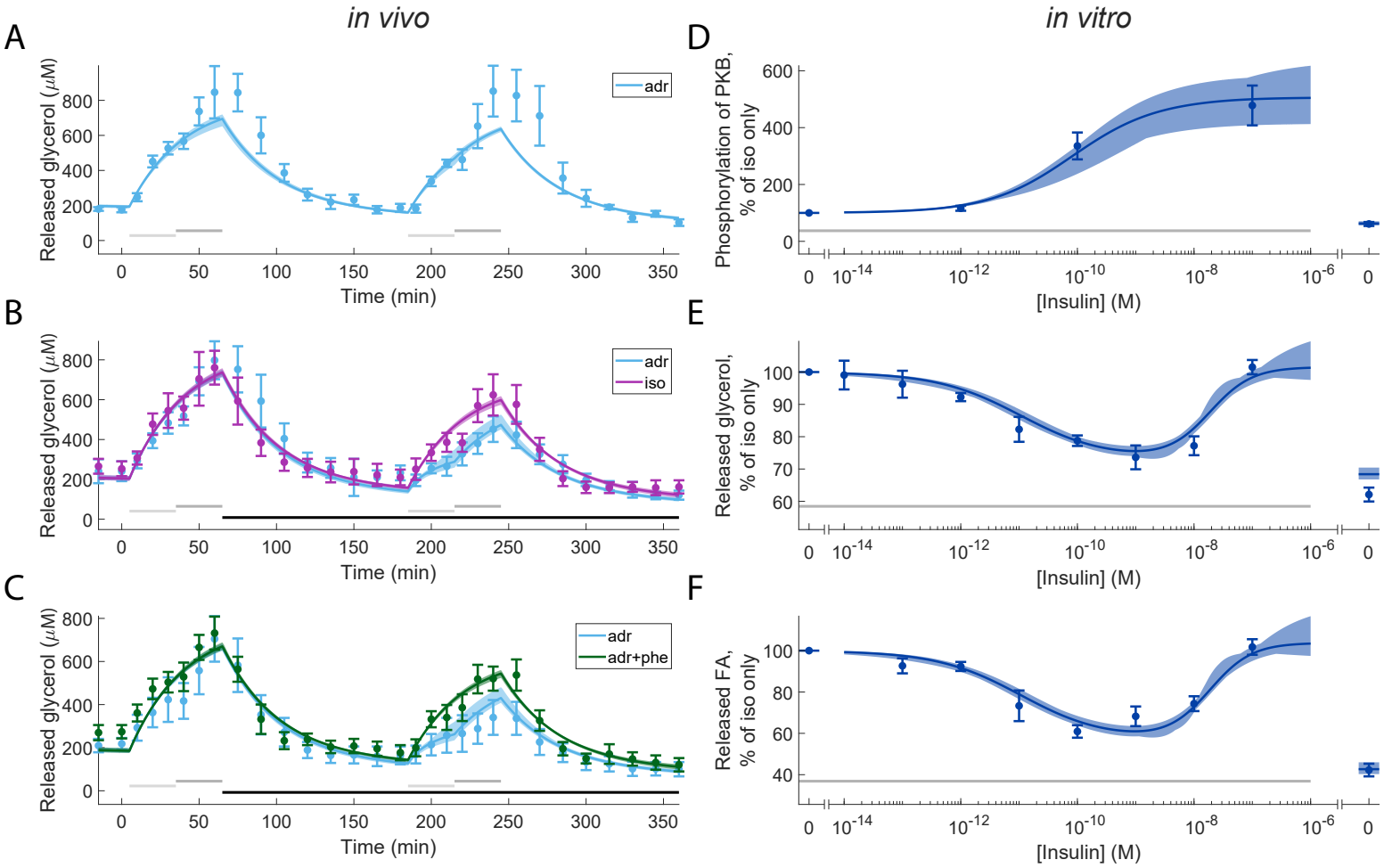

Figure S1: Model agreement to the measurables in the extended pool of experimental data not shown in Fig. 3. Estimation data and model simulations, for the original data (e.g. used in Fig. 2). In all panels, solid lines represent the model simulation with the best agreement to data, the shaded areas represent the model uncertainty, and experimental data point are represented as mean values with error bars (SEM). (A-C) are the *in vivo* time-series experiments, and (D-F) the *in vitro* dose-response experiments. In (A-C), horizontal light/dark grey lines represent stimulation with low/high adrenergic stimulus (1/10 μM adrenaline or 0.1/1 μM isoproterenol) with or without phentolamine (phe; 100 μM), horizontal black lines represent stimulation with insulin (0.6 nM) and in (D-F) horizontal grey lines represent simulation with isoproterenol (10 nM). In the *in vivo* experiments, experiments with adrenaline are shown in light blue (A-C), with isoproterenol in purple (B), and with the combined stimulation with adrenaline and phentolamine in green (C). In the *in vitro* experiments (D-F), increasing doses of insulin (x-axis) were given together with 10nM isoproterenol in all points except one. The point without isoproterenol got no stimulus and is shown to the right in the graphs. For full experimental details, see [4] for the *in vivo* experiments, and [3] for the *in vitro* experiments.

Parameter	lower bound	upper bound
$kdrift$	10^{-5}	10^{5}
$k1a$	10^{-5}	10^{5}
$k1a2$	10^{-5}	10^{5}
$k1b$	10^{-5}	10^{5}
$k2a1$	10^{-5}	10^{5}
$k2b$	10^{-5}	10^{5}
$k4a$	10^{-5}	10^{5}
$k4a2$	10^{-5}	10^{5}
$k4b$	10^{-5}	10^{5}
$k3a$	10^{-5}	10^{5}
$k3b$	10^{-5}	10^{5}
$k5a$	10^{-5}	10^{5}
$k5b$	10^{-5}	10^{5}
$k6basal$	10^{-5}	10^{5}
$k6a$	10^{-5}	10^{5}
$k6b$	10^{-5}	10^{5}
$k6b2$	10^{-5}	10^{5}
$k7a$	10^{-5}	10^{5}
$k7b$	10^{-5}	10^{5}
$k8a$	10^{-5}	10^{5}
$k8b$	10^{-5}	10^{5}
$k8c$	10^{-5}	10^{5}
$isoscale$	0.1	100
min_1	0	100
min_2	0	100
min_3	0	100
$EC50_1$	0.5	1.1
$EC50_2$	10^{-10}	10^{10}
$EC50_3$	10^{-10}	10^{10}
n_1	0	10
n_2	0	10
n_3	0	10

Table S1: All bounds used for the free parameters. The rate parameters (kx) were given a free range (10^{-5},10^{5}). $isoscale$ was allowed tenfold range from the expected value of 10. For the input functions, the minimum values min_x was given a range from zero to max (0,100), and the steepness $_x$ (0,10), and the $EC50_x$ was given a free range for all doses (10^{-10}, $10^{1}0$) nM, except for $EC50_1$ which was limited based on the EC50 of IR in [5].